Ultrafast fabrication of Nanofiber-based 3D Macrostructures by 3D electrospinning

Materials & Design 208 (2021) 109916

Contents lists available at ScienceDirect

Materials & Design

journal homepage: www.elsevier.com/locate/matdes

Ultrafast fabrication of Nanofiber-based 3D Macrostructures by 3D electrospinning

Michel Vong [a,*], Francisco Javiez Diaz Sanchez [a], Antonios Keirouz [a], Wiwat Nuansing [b,c], Norbert Radacsi [a,*]

[a] School of Engineering, Institute for Materials and Processes, The University of Edinburgh, Sanderson Building, King's Buildings, Edinburgh EH9 3FB, United Kingdom
[b] School of Physics, Institute of Science, Suranaree University of Technology, Thailand
[c] SUT CoE on Advanced Functional Materials (SUT-AFM), Suranaree University of Technology, Thailand

HIGHLIGHTS

- Various polymers and shapes can be built with the 3D electrospinning technology.
- The mechanism behind 3D build-up has been analyzed and characterized thoroughly.
- The shaping of 3D electrospun structures can be further enhanced with electrodes.
- The shelf-life and compressibility of the 3D structures have been characterized.
- The upscaling of 3D electrospinning, in term of size and quantity, has been achieved.

ARTICLE INFO

Article history:
Received 12 February 2021
Revised 10 June 2021
Accepted 16 June 2021
Available online 21 June 2021

Keywords:
3D electrospinning
Formation mechanism
Upscalability
Polystyrene
Polyacrylonitrile
Polyvinylpyrrolidone

ABSTRACT

Fabrication of macroscopic three-dimensional (3D) structures made of nanofibers of widely used polymers is reported. 3D structures have several benefits over conventional flat two-dimensional (2D) structures by the added dimension. The structures have been fabricated by the 3D electrospinning technology that can build 3D structures rapidly due to certain additives in the solution and appropriate process conditions. The process parameters of 3D electrospinning have been identified and investigated to better understand the formation mechanism of the 3D build-up for polystyrene (PS), polyacrylonitrile (PAN), and polyvinylpyrrolidone (PVP). Different types of electrodes were inserted in the electrospinning chamber to alter the electric field and have better control over the shape of the 3D structure. The upscalability of this technology was investigated by using a standard electrospinner and a nozzle-free electrospinning setup. It was possible to manufacture 3D structures with these devices, highlighting the versatility of this technology. 3D electrospinning opens the pathway for the facile fabrication of macroscopic 3D structure with microfibrous features on a commercial scale.

1. Introduction

Electrospinning is a versatile and simple technology that uses high voltage to draw micro- and nano-fibers from polymer solutions. By tuning the electrospinning parameters as well as the polymer solution properties, it is possible to have wide control over the shape and morphology of the fibers. The fibers' diameter, length, surface roughness, porosity, pore interconnectivity, degree of fibers alignment, beads-in-fibers are all controllable properties that can shape the desired fiber configuration [1-7]. Different types of fibers, such as hollow, core–shell, multichannel, branched, peapod or wire-in-tube are also obtainable structures [8-13]. Coupled with the ability to add functional nanoparticles or manufacture metallic or ceramic fibers [14,15], electrospinning can be purposed for a wide range of applications.

Recently, the electrospinning of unorganized three-dimensional (3D) structures has sparked interest as 3D structures offer some benefits over conventional two-dimensional non-woven electrospun structures. The 3D nature of the electrospun structure can allow it to be more moldable and to be easily fitted into particular locations; for instance, it can be used as a sealant to block leakage in tubing systems [16]. In energy storage and conversion, the use of a 3D carbon nanofibrous structure showed higher elasticity, higher durability and better performance than standard two-dimensional (2D) configurations [17]. This is due to the strong interconnection between the carbon fibers and the graphene additives, which

* Corresponding authors.
E-mail addresses: michel.vong@ed.ac.uk (M. Vong), n.radacsi@ed.ac.uk (N. Radacsi).

https://doi.org/10.1016/j.matdes.2021.109916
0264-1275/

create a conductive network. The high surface area and the multiple macropores help to enhance the electrochemical performance of the 3D structure. The highly porous network of a 3D structure can also offer better thermal insulation properties [18], as well as better oil-sorption capacity [19]. In the bioengineering field, 3D electrospun structures are typically used as scaffolds, as it can mimic the structure of the natural extracellular matrix [20,21]. With higher porosity and surface area as well as better control of the surface roughness, 3D electrospun structures can show better cell growth, attachment, viability and infiltration behavior than flat electrospun mats [22]. It was demonstrated in another work that combining a 3D structure with aligned fibers can favor tissue growth in a preferential direction [23]. 3D fibrous structures have also shown stronger mechanical stability, and better transport pathway for electrons and ions, which is desirable in energy storage applications [24,25]. Combining 3D features with existing nanofibrous structures in energy devices could potentially increase their efficiency [26,27].

There are multiple methods to induce the formation of 3D structures through electrospinning [28,29]. A few examples of these methods are electrospinning onto 3D printed collectors [30], freeze-drying of electrospun fibers in a mold to shape a 3D structure [31] or gas-foaming to expend the electrospun mat [32]. Nevertheless, the simplest techniques to build 3D structures through electrospinning is direct self-assembly of the electrospun polymer [33]. This technique can typically build the 3D structure in a single step, in about 10 min of electrospinning. Multiple studies have shown that the incorporation of additives is critical to force the electrospinning of 3D structures using this method. However, most theories trying to explain the formation mechanism of the 3D electrospun structures are mostly speculative and do not rely on quantitative measurements. Another weakness of the previous studies is that there is no control over the final shape of the 3D structures, which leads to poor reproducibility of the buildup [34]. Self-assembly of the electrospun polymer is also sensitive to the relative humidity, which needs to be set in a precise range to force the buildup [35]. To alleviate these issues, a novel and simple technology called 3D electrospinning has been developed [36]. While the initial results showed precise control over the shaping of the 3D electrospun structure, no quantitative analysis was performed to explain the formation mechanism of the 3D buildup, and the buildup was only shown on a single polymer system, which would limit the range of application of this technology.

The present work sheds light on several factors in 3D electrospinning that can induce 3D build-up of nanofibers such as viscosity of the polymer solution, interaction between additive and polymer system, crystallinity of the electrospun fibers and polymer solution conductivity. The effect of different types of electrodes on the electric field is also investigated in an attempt to obtain better control over the electrospinning jet, and ultimately, the shape of the electrospun 3D structure. Finally, this paper highlights the versatility of the 3D electrospinning technology by successfully electrospinning 3D structures using several polymers. The upscalability of the 3D electrospinning process, using a high-throughput nozzle-free electrospinning setup, and the long-term stability of the 3D structures is further investigated.

2. Materials and methods

2.1. Materials

The polymer polystyrene (PS) was acquired from Sigma-Aldrich, polyacrylonitrile (PAN) was purchased from Shandong Jianuofu Treasure Industrial Co., Ltd (Jinan, China) and polyvinylpyrrolidone (PVP) was obtained from Alfa Aesar. The average molecular weights (Mw) were 280000, 150000, 360000 $g.mol^{-1}$ for PS, PAN and PVP respectively.

The solvent N,N-dimethylformamide (DMF) (greater than99.9% purity) was purchased from Sigma-Aldrich, tetrahydrofuran (THF) (99+% purity, stabilized with butylated hydroxytoluene) was acquired from Acros Organics and methanol (MeOH) (≥99.9% purity) was obtained from Fisher Scientific.

Hydrochloric acid (HCl) (37% solution in H_2O) was acquired from Sigma-Aldrich, phosphoric acid (H_3PO_4) (85% solution in H_2O) was purchased from Acros Organics, while formic acid (HCOOH) (98/100% purity) and sulphuric acid (H_2SO_4) (greater than95% purity) were both received from Fisher Scientific. Ammonium hydroxide (NH_4OH) (28% NH_3 in H_2O) was obtained from Alfa Aesar, and the sodium hydroxide (NaOH) pellets (99.59% purity) was purchased from Fisher Scientific.

2.2. Solution preparation

The polymers were dissolved in their respective solvent by stirring at ambient conditions. All concentrations are given in weight percentage (wt%). PS 15 wt% was dissolved in DMF, PAN 15 wt% was dissolved in DMF, and PVP 15 wt% was dissolved in MeOH. The additives, if any, were inserted after complete dissolution of the polymer solution. The amount of additives inserted was between 2 μL and 200 μL per 20 g solution. Each electrospinning experiment lasted 10 min and was performed using a "fresh" polymer solution.

To prepare 37% NaOH solution, 3.7 g of NaOH were mixed in 6.3 g of H_2O and stirred until complete dissolution. All other products were used without any further purifications.

2.3. Electrospinning apparatus

The first electrospinning apparatus combines a 3D printer with electrospinning, referred to as "3D electrospinning", throughout this work. As such, it is possible to control the movement of the nozzle and thus, the location of the fibers deposition area during electrospinning. The apparatus itself (NovaSpider, CIC nanoGUNE, Spain), seen in Fig. 1(a-b), is made of a syringe pump, a nozzle connected to two conveyor belts (x- and y-axis movement), a vertically-moving platform as the collector (z-axis movement), and a high voltage DC power supply. The two conveyor belts allow for the movement of the nozzle head in the x-y plane, with a resolution of 0.02 mm. The motion pattern imposed to the nozzle head in this work was a 5.5 cm circle. The nozzle head had a moving speed of 12.0 $mm.s^{-1}$. The voltage applied at the nozzle head was set to 20 kV. The collector, wrapped in aluminum foil, was set to a working distance of 5 cm. The collector is connected to a −5 kV DC power supply (HV050REG(-), Information Unlimited, Amherst, USA), which acts as the ground. The pump flow rate was set to 5 $mL.h^{-1}$, unless stated otherwise. The syringe needle used had a gauge of 20 G (inner diameter 0.603 ± 0.019 mm).

This setup was also used in stationary mode, with an immobile nozzle and collector, and constant applied high voltage and flow rate. The purpose of the stationary mode is to have a comparative study with the conventional electrospinning process.

The second apparatus is a custom-made needleless electrospinning device, as shown in Fig. 1(c-d). The setup consists of a polymer solution bath, a stainless-steel cylinder submerged within the bath to generate fibers and a metallic drum that acts as a collector for the fibers. The polymer solution bath is made of Teflon® (PTFE) and has a volume of 9 cm × 3 cm × 2 cm. The fiber-generating cylinder has a diameter of 3 cm and is fitted with a 12 V DC motor (6 $N.cm^{-1}$, 4500 rpm, Bosch, Gerlingen, Germany) that allows rotations at a constant speed of 10 RPM. The collector cylinder has a diameter of 6 cm, covered in aluminum foil and fitted to a 12 V

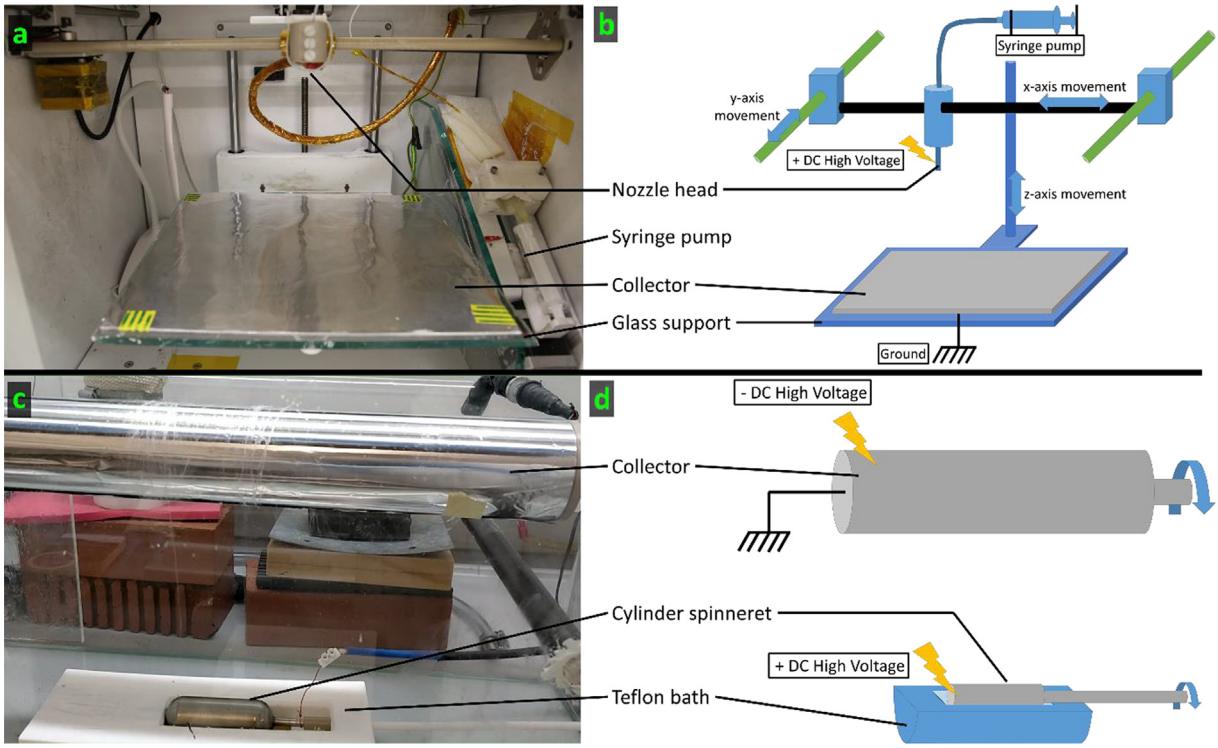

Fig. 1. The electrospinning apparatuses. (a) Photograph of the 3D electrospinning setup, and (b) schematic drawing. (c) Photograph of the nozzle-free electrospinning setup and (d) schematic drawing.

DC motor (15 N.cm, 6 rpm, RS PRO, United Kingdom) powered by an adjustable power supply (DPPS-16–30, VOLTCRAFT, Hirschau, Germany). During electrospinning, the rotation speed was either set to 30 RPM or left at 0 RPM while adjusting the deposition area every 2 min. The distance between the stainless-steel spinneret and the collector was set at 15 cm. A + 35 kV (HV350REG(+), Information Unlimited, Amherst, USA) and a −35 kV (HV350REG(-), Information Unlimited, Amherst, USA) high voltage DC power supply were used to charge the spinneret in the polymer solution bath and the collector, respectively. As the polymer solution bath is placed below the collector, the fibers are produced in an upward motion. 3D structures were obtained with PS by applying + 25 kV at the polymer bath and −15 kV at the collector and with PAN by using + 20 kV to charge the polymer bath and −15 kV to the collector. This setup was used to study the versatility of the 3D electrospinning process.

All electrospinning experiments were carried out at ambient conditions. The temperature was between 20 and 25 °C, and the relative humidity ranged between 35 and 45%. These were measured for each experiment using a digital thermohydrometer (HTC-1, HTC Co., Ltd, New Taipei City, Taiwan).

2.4. Modification of the electric field

Different conductive obstacles and support material were put in the electrospinning chamber to modify the path of the electrospun jet. These objects were custom made with cardboard wrapped in aluminum foil and have the shape of a flat circle, ring or flat rectangles. They were placed either at the nozzle level or on the collector so that they could act as the base, steering or guiding electrodes. The base electrodes were a 5 cm circle, a 10 cm circle and a 5.5 cm ring placed around the nozzle. The steering electrode was a 5.5 cm floating ring placed mid-way between the nozzle and the collector. The guiding electrodes were two 4 cm × 5 cm rectangles and a 5.5 cm ring placed on the collector. All electrodes configurations used are summarized in Fig. 2.

2.5. Characterization

2.5.1. Digital imaging

All pictures of the 3D macroscopic shapes after electrospinning were taken using a digital camera (EOS 6D, Canon Inc., Tokyo, Japan). Recorded videos of the electrospinning process were taken with the same digital camera or using a OnePlus 5 dual camera (One Plus Technology, (Shenzhen) Co., Ltd., Shenzhen, China).

A high-speed camera (FASTCAM SA6, Photron, Tokyo, Japan) was used to obtain high precision images of the electrospun jet during 3D-build-up. The high-speed camera was set to a resolution of 768 × 512 pixels and a framerate of 10,000 FPS. The electrospinning jet was illuminated from the front with a lamp head (Multi-LED LT, GS Vitec GmbH, Bad Soden-Salmünster, Germany). The whipping angle of the jet was measured with the image processing program Fiji-ImageJ (v.1.52, National Institutes of Health, Bethesda, USA), by using 3 frames of the recorded electrospinning process.

2.5.2. ***Scanning*** *electron* ***microscopy***

The samples were analyzed with a scanning electron microscope (SEM) (JEOL JSM-IT100, JEOL Ltd., Tokyo, Japan). The shape and size of the electrospun fibers were further characterized using the image processing program Fiji- ImageJ. More than 100 fibers per sample were used to obtain the mean diameter of the fibers. All samples were sputter-coated (Desk III, Denton Vacuum, Moorestown, USA) with approximately 10 nm of Gold prior to observation.

2.5.3. Compression ***tests***

Weights of 10.0, 20.0 and 50.0 g (A.H. Baird, Edinburgh, United Kingdom) were used to perform compression creep tests on the

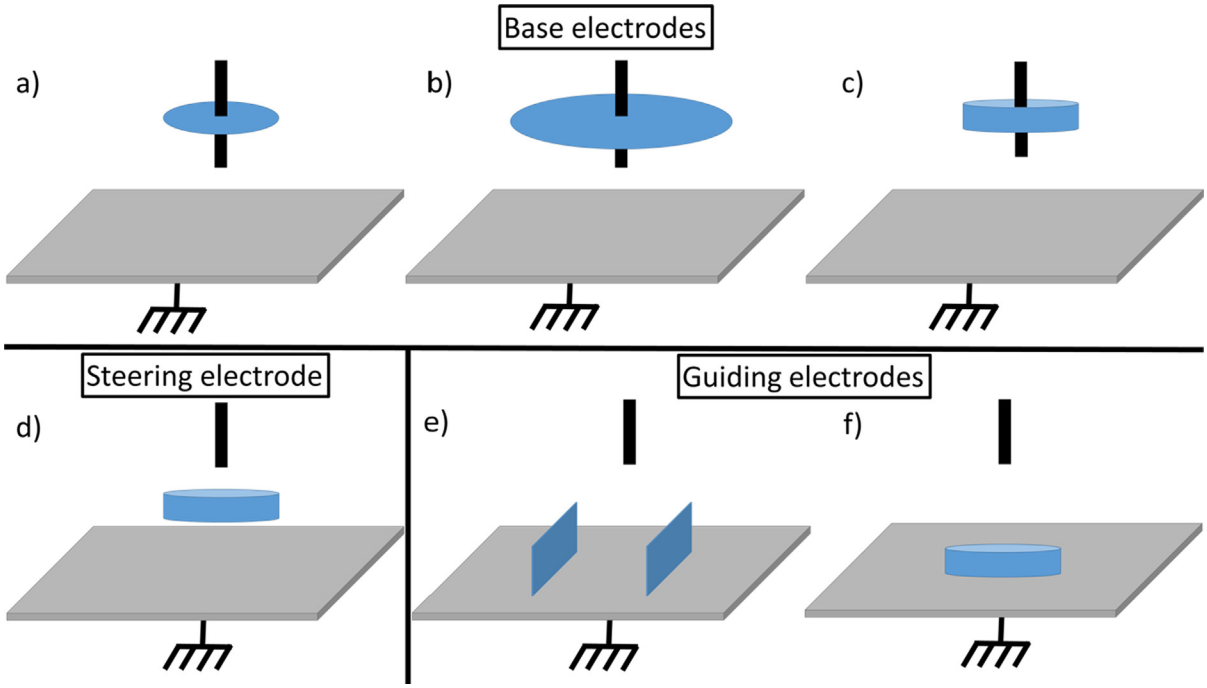

Fig. 2. Schematics of the used electrode configuration used. Base electrodes, with (a) being a 5 cm circle around the nozzle, (b) a 10 cm circle around the nozzle, (c) a 5.5 cm ring around the nozzle. (d) is a steering electrode in the shape of a 5.5 cm floating ring, and is placed 2.5 cm above the collector. Guiding electrodes with (e) two 4 cm × 5 cm rectangles and (f) a 5.5 cm ring on the collector.

electrospun 3D structures. The weights were put on a 10 pence coin (~6.5 g) on top of the 3D structure to ensure a similar surface area was compressed for all weights. These tests were done on "fresh" 3D electrospun samples, with no additional treatment. Compression creep tests were performed over a total of 20 days to observe the long-term deformation of the 3D structures.

2.5.4. Rheology

The zero-shear viscosity was estimated by extrapolation using a rotational rheometer (MCR 302, Anton Paar, Graz, Austria) with a cone-plate configuration (diameter: 25 mm - gap: 0.1 mm). All samples were pre-sheared at a constant shear rate of 1 s^{-1} for 1 min before the actual analysis. A shear rate sweep test was then performed from 500 to 1 s^{-1}. The temperature of the cone and plate were kept constant at 23 °C.

2.5.5. ***Fourier-transform infrared*** *spectroscopy* ***(FTIR)***

The measurements were performed using a spectrometer (Varian 640-IR, Varian Medical Systems, Palo Alto, USA) in ATR (Attenuated Total Reflection) mode in the scanning range 4500–600 cm^{-1}, with a spectral resolution of 2 cm^{-1}, where the sum of 32 scans were obtained per specimen.

2.5.6. X-ray diffraction (XRD)

The measurements were carried out with a benchtop XRD system (Bruker D2 PHASER, Bruker, Billerica, USA). Scans were performed using Cu Kα radiation over a 2θ range of 5° to 60°, at a step size of 0.05° and a scanning rate of 6°.min^{-1}.

2.5.7. ***Differential scanning*** *calorimetry* ***(DSC)***

The measurements were obtained using a calorimeter (DSC 204 Instrument, Netzsch, Selb, Germany) under nitrogen atmosphere (50 mL.min^{-1}), on at least 5 mg of sample in an aluminum pan. The samples were first cooled from 40 °C to 20 °C and then subjected to three cycles of heating from 20 °C to 280 °C and subsequently brought back to 20 °C. The heating and cooling rates were 10 °C.min^{-1}.

2.5.8. Polymer solution conductivity measurements

After complete dissolution of the polymer solution, its conductivity was measured using a glass probe conductivity meter (Traceable™, Fisher Scientific, Pittsburg, USA). The probe was dipped in the respective organic solvent of the polymer solution before measurement, at ambient conditions.

2.5.9. ***Electric field*** *simulations*

The simulations of the electric field generated by the different electrodes system were performed with a finite element simulation software (v5.3a, COMSOL Multiphysics, COMSOL Inc, Burlington, USA). The AC/DC module of COMSOL was used to simulate the 3D electric field. The nozzle head was designed as a hollow steel cylinder of 20 mm height, 0.5140 mm inner diameter and 0.8192 mm outer diameter. Then, a voltage of 20 kV was simulated onto the nozzle head. The collector was a 26 cm high, 20 cm wide and 0.5 cm thick aluminum rectangle, defined as ground (no voltage applied). The various electrodes presented the same dimensions as defined previously and were simulated as aluminum material. The base electrodes were given a voltage of 20 kV as they were in contact with the nozzle while the guiding electrodes were defined as the ground, along with the collector. The boundary domain was a 31 cm high, 25 cm wide and 10 cm thick rectangle. The final geometry was built with a "Fine" mesh size.

3. Results and discussion

3.1. 3D electrospinning of polystyrene, polyacrylonitrile and polyvinylpyrrolidone

Large 3D electrospun structures of polystyrene (PS), polyacrylonitrile (PAN) and polyvinylpyrrolidone (PVP) were fabricated to

show the versatility of polymers that can be used for 3D electrospinning. The fabrication of electrospun 3D PS structures has been reported in previous papers [36,37]. There were differences observed in the 3D shape and final height between each polymer.

As can be seen in Fig. 3, the PS structure is the only one that can follow the circular pattern of the nozzle head and have the shape of a cylinder. It has a height of 3.0 ± 0.1 cm and an average wall thickness of 2.4 ± 0.1 cm. The PAN 3D structure has the shape of a cone, 3.2 ± 0.1 cm in height, with a base thickness of 11.6 ± 0.2 cm and a top thickness of 3.1 ± 0.1 cm, and the PVP structure is made of several small cones, with a bigger one of 1.1 ± 0.1 cm in height, 4.5 ± 0.1 cm in base thickness and 2.0 ± 0.1 cm top thickness, located in the center of the electrospinning area. The circular motion of the nozzle forces the center of the electrospinning area to be continuously exposed to the electrospinning jet, which explains why the central cone is larger. The average fiber diameters were 0.85 ± 0,02 μm, 0.74 ± 0.01 μm and 1.04 ± 0.2 μm for PS, PAN and PVP, respectively. In the present study, the electrospinning time was set to 10 min, which translates to a layering speed of about 0.3 cm.min^{-1} for PS and PAN. As a comparison, technologies such as direct-write melt electrospinning typically build 3D structures up to 7 mm while near-field electrospinning has been reported to have a layering speed of 30 μm.s^{-1}, able to stack 800 layers of fibers to build a 1.3 cm tall hollow cylinder [38-40]. 3D printing, a rapid prototyping technology, has been reported to stack layers at a speed of 0.4 mm.min^{-1} [41]. This highlights the ultrafast fabrication of the 3D electrospinning technology.

The difference in shape between PS, PAN and PVP structures can be explained by observing the wider whipping motion of the PAN and PVP jets, which lead to a higher deposition area and less control over the shaping of the 3D structures. Indeed, the whipping angle of the jet was measured to be 85 ± 1°, 113 ± 1° and 125 ± 1° for PS, PAN and PVP respectively, as shown in Fig. 3. That comes into correlation with the increased polymer solution conductivity measured at 80.4 ± 0.8 μS.cm^{-1}, 1.05 ± 0.01 mS.cm^{-1} and 4.16 ± 0.04 mS.cm^{-1} for PS, PAN and PVP respectively. As shown in previous research, an electrospun jet with more charge carriers is more susceptible to the external electric field and surface charge repulsion, which can, in turn, lead to a wider whipping motion [42-44].

Another interesting observation is the shape of the PVP Taylor cone, which is an elongated droplet of about 1 cm in length. This peculiar shape is most likely due to the relatively high conductivity of the PVP solution and the high flow rate used for inducing 3D electrospinning. Previous research has shown the detrimental effect of high conductivity in the polymer solution [45]. While it is necessary to increase the surface charge density to induce the formation of the Taylor cone, a conductivity too high can decrease the electric forces at the surface of the droplet which hinders electrospinning [29,45]. Likewise, a high flow rate can also lead to a lower surface charge because of the increased amount of polymer supplied [46]. At high flowrate, aggregation of the fluid can occur at the tip of the nozzle head, which is usually followed by dripping of the polymer solution [47]. In this study, partial drying of the PVP polymer solution at the nozzle head was observed during electrospinning, possibly due to the high evaporation rate of methanol. This might prevent dripping as well as help initiate the Taylor cone for electrospinning. No dripping of the PVP polymer solution is observed during the 10 min of 3D electrospinning.

3.2. Physical stability of 3D electrospun structures

The long shelf-life property of electrospun 3D PS has been previously reported [36]. 3D PAN is also observed to have a long shelf-life and is stable for more than 12 months at ambient conditions. 3D PVP, being a water-soluble polymer, is sensitive to the ambient humidity [48,49]. Collapse of the 3D PVP features and partial dissolution of the structure have been observed after a few months in the lab. As such, this present study focuses on the effect of compressive forces on the shape recovery of these electrospun 3D structures.

Electrospun 3D PS demonstrates partial shape recovery on short-term (5 min) compressive strength, developing a strain of about 20–30%. This is true for all 3 weights examined: 10.0, 20.0 and 50.0 g. For all weights, it is observed that most of the deformation occurs within the first two hours; getting as high as 51.9%,

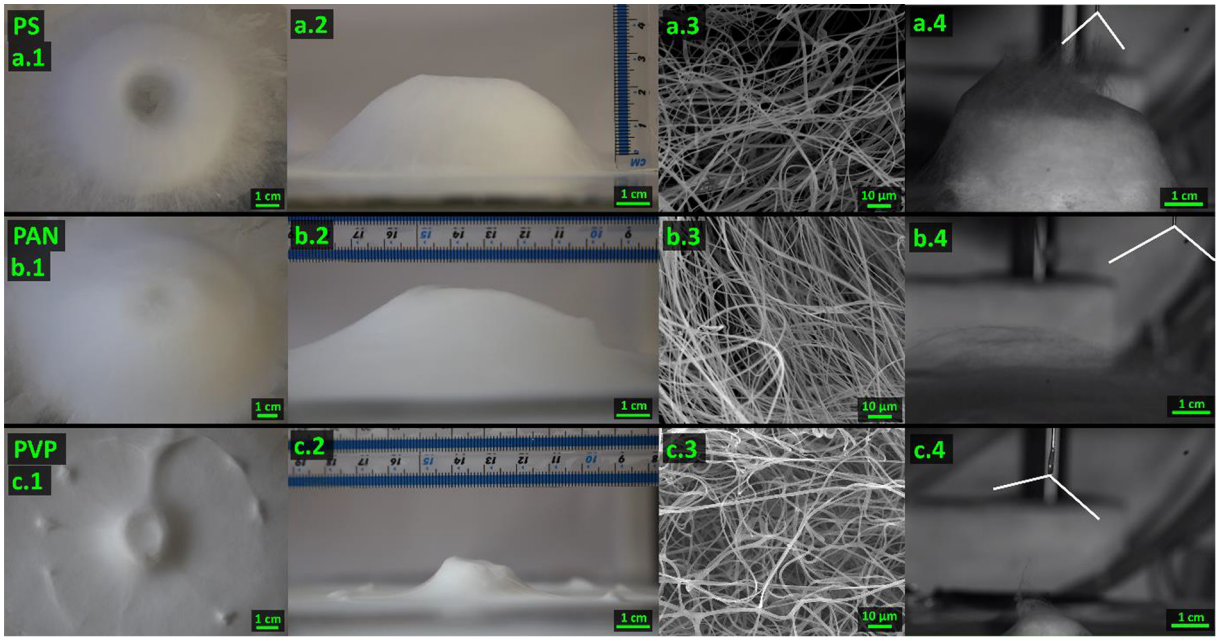

Fig. 3. 3D electrospun structures of PS, PAN and PVP. (a.1) Top-view, (a.2) Side view, (a.3) SEM pictures and (a.4) High FPS camera picture during electrospinning of 3D PS. (b.1), (b.2), (b.3) and (b.4) are for 3D PAN. (c.1), (c.2), (c.3) and (c.0.4) are for 3D PVP.

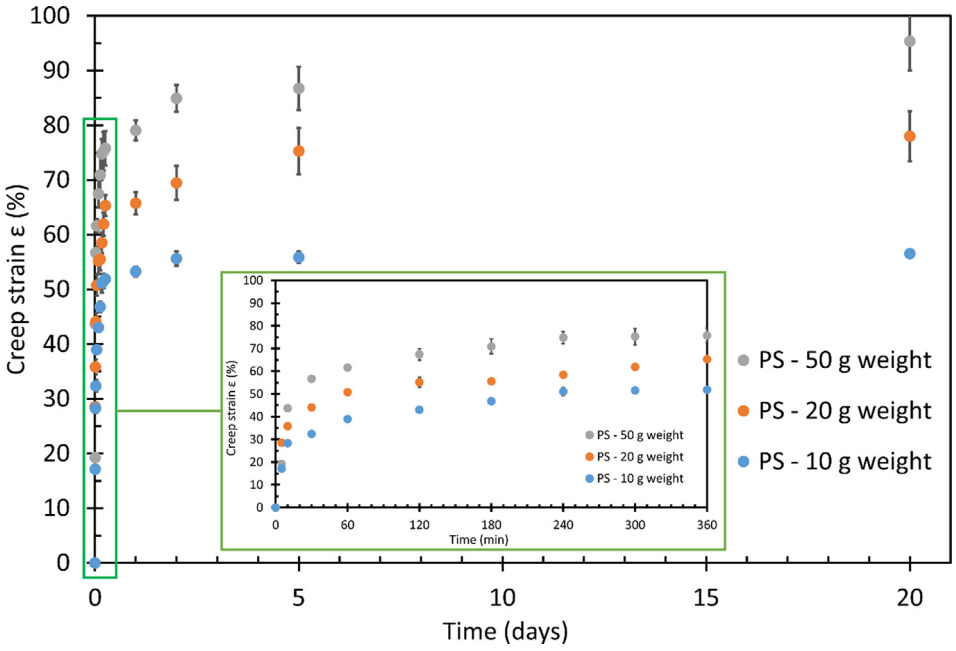

Fig. 4. Compression creep test on electrospun 3D PS. Most of the creep deformation is observed within the first 6 h of loading, getting a deformation as high as 51.9%, 65.3% and 75.8% for the weights of 10, 20 and 50 g respectively.

65.3% and 75.8% after 6 h of compression for the weights of 10.0, 20.0 and 50.0 g, respectively. A total strain of about 56.6%, 78.0% and 95.4% is observed for the same respective weights after 20 days of constant loading. This multiple-stage deformation behavior is typical in the compression creep test of polymeric material [50,51]. It is due to the densification of the fibers, which increases their mechanical strength and resistance to compression [16,52]. The results of the compression creep test can be seen in Fig. 4.

Electrospun 3D PAN and 3D PVP structures, while also showing relatively long shelf-life, have no elasticity and permanently lose their 3D feature after a light compression, as seen in Figure S1. This is because PAN can retain its charge over a long time, and these residual charges make the PAN fibers attracted to the weight, skewing the effect of a compression load on the 3D PAN structure [53]. PVP itself is known for its adhesive properties, which would prevent it from regaining its former height [54,55].

3.3. Investigation on the 3D electrospinning formation mechanism

3.3.1. Viscosity of the polymer solution

The viscosity of the polymer solutions was measured before and after inserting the HCl additive. HCl, when inserted in the correct concentration, is an additive prone to promote 3D electrospinning in the 3 different polymer system studied. As seen in Fig. 5, the additive does not cause any significant difference in the shear viscosity despite the 3D nature of the electrospun product. In more details, the zero-shear viscosity of 15 wt% PS in DMF is of about 9.5×10^1 mPa.s, with or without additives. 15 wt% PAN in DMF is at about 2.3×10^3 mPa.s and 15 wt% PVP in MeOH stays at about 1.6×10^2 mPa.s. All of these viscosity values are in a similar range than previous researches [56-58]. The negligible gap measured with additive is attributed to the preparation method of the polymer solution, which slightly alter the polymer concentration. This

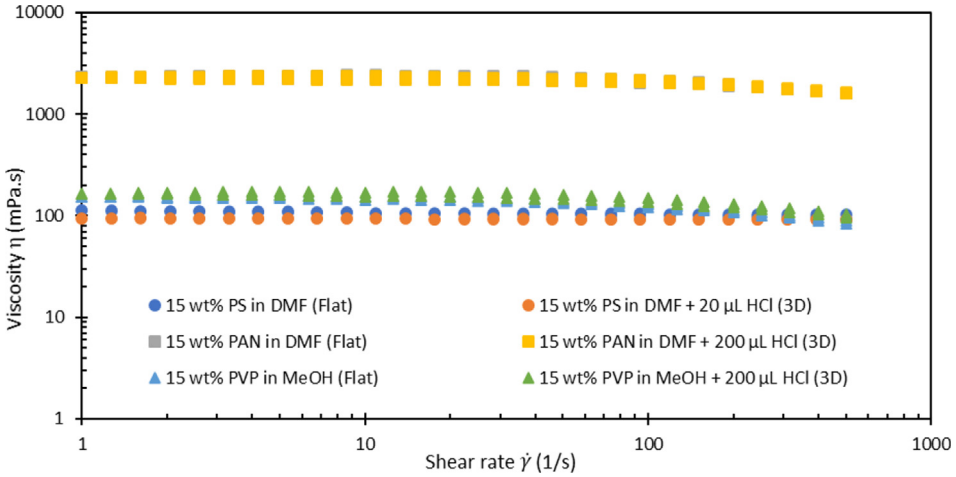

Fig. 5. The viscosity of polymer solutions with (3D) and without (flat) HCl additive. The symbols; (●)15 wt% PS in DMF with and without HCl (■) 15 wt% PAN in DMF without and with HCl (▲) 15 wt% PVP in MeOH without and with HCl. There is no significant change in viscosity with additives.

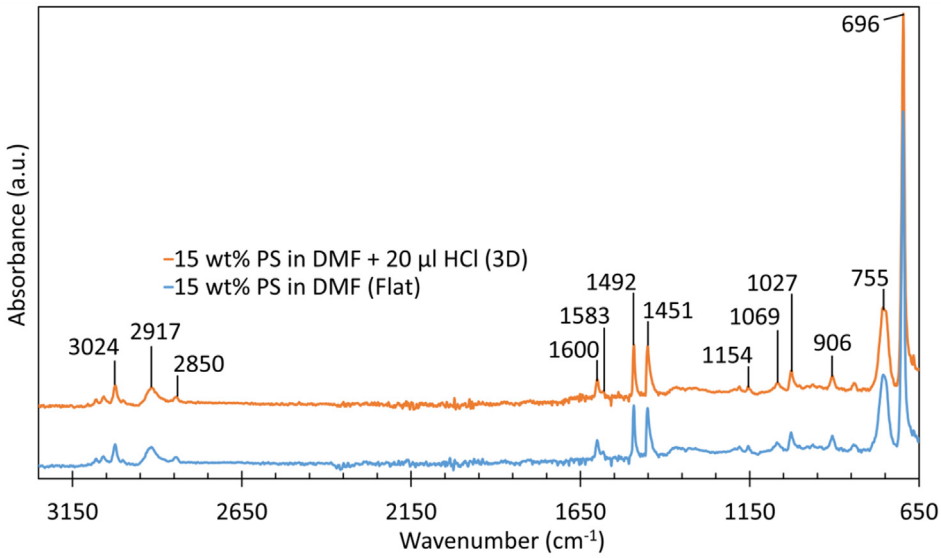

Fig. 6. FTIR spectra of electrospun PS fibers, with (3D) and without (flat) HCl additive. No significant shifts in peaks are observed.

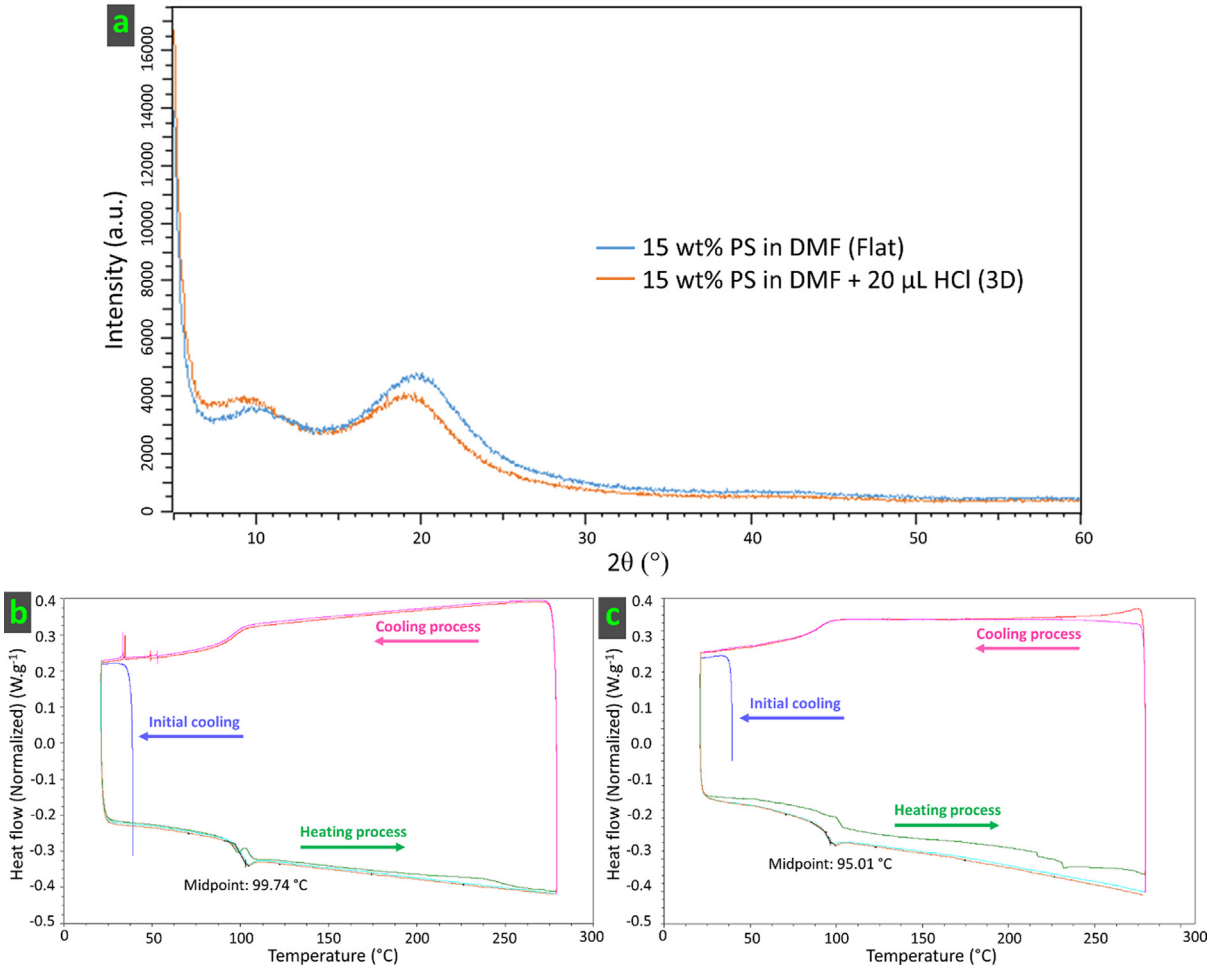

Fig. 7. (a) XRD patterns of electrospun PS fibers, with (3D) and without (flat) HCl additive. No significant differences were observed between the two samples. DSC thermograms of PS with 3 cycles of heating–cooling (b) Pristine PS and (c) Electrospun 3D PS. The thermal behavior of these two samples is similar.

lack of difference is a clear indication that the viscosity does not play a major role in the elaboration of 3D electrospun structures. This result is in direct contradiction with the hypothesis proposed by Li M. et al., who speculated that the increased viscosity of their PVP solution after adding $Fe(NO_3)_3$ was the main cause of the 3D build-up during electrospinning [34].

3.3.2. Chemical interactions between additive and polymer

In this study, FTIR spectra of 2D and 3D PS fibers were examined to evaluate if there were major differences caused by the insertion of the additive responsible for the 3D build-up. As seen in Fig. 6, the weak adsorption peaks at about 3024 cm^{-1} are due to the C-H stretching of the benzene ring of PS. The C-H stretching of the CH_2 and CH groups of the main PS chain is typical of the weak absorption bands at around 2917 and 2850 cm^{-1}, respectively. Benzene ring vibrations are observed at the frequencies 1600 and 1583 cm^{-1}, as well as with the strong peaks at 1492 and 1451 cm^{-1}. The small peak at 1154 cm^{-1} is due to C-H bending, in *para*-position. The moderate peaks at 1069 and 1027 cm^{-1} are due to hydrogen-bending modes in the benzene ring. Lastly, the less intense peak at 906 cm^{-1} and the strong peaks at 755 and 696 cm^{-1} are due to out-of-plane C-H bending. As for the main PS chain itself, the stretching mode and bending mode of CH_2 are mixed within the bands at 2917 and 1451 cm^{-1} respectively, and C-C stretching is mixed with the 1069 cm^{-1} band [59-62].

After identifying the characteristic peaks of PS, it is concluded that there were no shifts of any major PS peaks between the flat and 3D FTIR spectra, and further, no additional peaks could be identified. As such, it is very unlikely that the additive would favor any kind of interaction between the polymer and the solvent system.

3.3.3. Crystallization of the electrospun fibers

In this study, the XRD pattern of flat and 3D PS has been analyzed, as well as their thermal behavior through DSC. It was postulated that the driving force of the 3D build-up was due to a change of crystallinity in the polymer fibers during electrospinning, which could be verified by looking at specific XRD peaks change or measuring the glass transition temperature.

In Fig. 7 (a), the XRD patterns of both the flat and 3D PS samples show broad weak peaks at 10° and 20°, which are indicative of low crystallinity level [62-64]. There are no significant differences between the two samples, either in additional characteristic peaks or in more intense peaks, which suggests a lack of effect of the acid additive on the crystallinity of the electrospun fibers. This result was further supported by the thermal analysis of the samples. The DSC curves of pristine PS and 3D PS, in Fig. 7 (b-c), show no significant change towards the thermal behavior of the material between the two forms. The glass transition temperature (T_g) was measured at 99.74 °C and 95.01 °C for pristine and 3D PS, respectively. This temperature comes in agreement with the expected range of previously published works [65-67]. In the cooling process, vitrification of both samples is observed near the T_g, which is typical of PS samples [68,69]. Neither sample shows any crystallization or melting point in this temperature range. The XRD and DSC results show there is little sign of crystallinity in the electrospun flat and 3D PS. As such, the driving force of the 3D build-up is not related to the *in-situ* crystallization of the polymer.

3.3.4. Solution conductivity

Several PS/DMF solutions with different amounts of acid or base additives were used to assess the effect of solution conductivity on the 3D build-up during electrospinning. As seen in Table 1, standard flat electrospinning is observed at solution conductivities of 0.24, 0.62, 3.15, 28.6, 32.3 and 48.0 $\mu S.cm^{-1}$, which were obtained by using no additives, by adding 20 µL of NH_4OH, 2 µL of HCl, 20 µL of HCOOH, 5 µL of HCl and 10 µL of HCl respectively. 3D electrospinning is achievable with solution conductivities of 4.04, 8.84, 32.2, 59.3, 73.1, 135.4, 140.3 and 206.0 $\mu S.cm^{-1}$, which were prepared by adding 20 µL of H_3PO_4, 40 µL of H_3PO_4, 20 µL of NaOH, 15 µL of HCl, 20 µL of HCl, 40 µL of HCl, 100 µL of H_3PO_4 and 20 µL of H_2SO_4 respectively.

Table 1
Polymer solution conductivity in the presence of various additives and whether 3D electrospinning was achieved or not. The electrospinning conditions were as follow: Applied voltage 20 kV, Working distance 5 cm, Flow rate 5 $mL.h^{-1}$.

15 wt% PS (Mw 280 k) in DMF				15 wt% PAN (Mw 150 k) in DMF				15 wt% PVP (Mw 360 k) in MeOH			
Additive	Amount (µL in 20 g of solution)	Conductivity ($\mu S.cm^{-1}$)	3D Build-up (Yes/No)	Additive	Amount (µL in 20 g of solution)	Conductivity ($\mu S.cm^{-1}$)	3D Build-up (Yes/No)	Additive	Amount (µL in 20 g of solution)	Conductivity ($\mu S.cm^{-1}$)	3D Build-up (Yes/No)
None	0	0.24	No	None	0	119	No	None	0	32.2	No
NH_4OH	20	0.62	No	HCl	200	1050	Yes	HCl	200	4.2×10^3	Yes
HCl	2	3.15	No								
H_3PO_4	20	4.04	Yes								
H_3PO_4	40	8.84	Yes								
HCOOH	20	28.6	No								
NaOH	20	32.2	Yes								
HCl	5	32.3	No								
HCl	10	48.0	No								
HCl	15	59.3	Yes								
HCl	20	73.1	Yes								
HCl	40	135.4	Yes								
H_3PO_4	100	140.3	Yes								
H_2SO_4	20	206.0	Yes								

While it is possible to sweep a wide range of conductivity from ~ 0.24 μS.cm^{-1} to ~ 140.3 μS.cm^{-1}, there is no direct correlation between 3D electrospinning and solution conductivity or a minimum solution conductivity before which 3D build-up initiates. As an example, 3D electrospinning is observed at solution conductivities of 4.04, 32.2 and 59.3 μS.cm^{-1} but not at the intermediate solution conductivities of 28.6 and 32.3 μS.cm^{-1}. As such, solution conductivity alone is not the driving factor of 3D electrospinning. Previous publications have shown that the outer surface of the deposited fibers is negatively charged due to polarization and electrostatic induction by the surrounding positive electric field [36,37]. These negative charges favor fibers repulsion, which lead to a 3D structure instead of a flat mat [70]. In particular, it is interesting to note that the 3D structures would be formed using HCl additives only after a minimal amount of HCl has been inserted; 15 μL in 20 g of PS solution. This can be because a high amount of charged particles would favor a strong polarization under the high electric field, which would increase the repulsive forces and the 3D buildup [37]. Rapid solidification of the fibers is also another factor that helps strengthen the 3D structure [71]. It is interesting to note that HCOOH and NH_4OH, a weak acid (pKa = 3.75 at 20 °C) [72] and a weak base (pKb = 4.767 at 20 °C) [73] respectively, are unable to induce 3D electrospinning to the PS/DMF solution. This may be due to the lower amount of ions they can provide to the solution. Indeed in another work, Yousefzadeh et al. used a deionizer to remove the extra charges from electrospun PAN, and that resulted in flattening of the fiber mat [74].

3.4. Electrospinning jet control

The 3D electrospinning setup used in this study allows for the fabrication of 3D electrospun structures with a wall thickness of ~ 1–2 cm. In order to have a better wall resolution, electrodes can be used to guide the electrospinning jet path and reduce the size of deposition area. Numerous studies have shown that the presence of these electrodes changes the shape of the electric field, which directly influence the electrospinning process. Depending on the position of the electrodes, the electrodes can serve different purposes [75,76]. If placed at the level of the nozzle head, they act as a base electrode, decreasing the size of the deposition area. If they are in the electrospinning pathway, between the nozzle and the collector, they are steering electrodes that control and deflect the trajectory of the electrospun jet. If located in the vicinity of the collector, they act as guiding electrodes, which serve as a converging area for the electrospun jet. In this study, base electrodes, steering electrodes and guiding electrodes have been used to attempt to electrospin 3D structures with better shape fidelity, most notably in the wall thickness. Previous studies on self-assembly of electrospun structures and 3D electrospinning

The base electrodes used were in the shape of a 5 cm circle, a 10 cm circle and a 5.5 cm ring. The base electrodes were shaped as flat circles as previous studies have shown these flat base electrodes were efficient in reducing the deposition area [77]. While a previous study by Yousefzadeh M. et al. has shown it was necessary to increase the applied voltage to induce the jet formation with a larger circle, a high voltage of + 20 kV was still sufficient to initiate electrospinning in our experiment [76]. Likewise, a ring electrode was chosen for its ability to stabilize the jet, direct it and decrease the deposition area [78]. All 3 shapes of base electrode used failed to electrospin uniform fibers and instead favored the formation of microbeads and dripping. As seen in Fig. 8, the base electrodes prevent the whipping motion of the electrospun jet and the linear jet experiences inadequate stretching and drying. This result can be explained with the work of Bunyan N. N. et al. and Yang Y. et al [79,80]. In their research, adding a base electrode at the nozzle level increased the linear jet section before the whipping motion and also decreased the deposition area on the collecting target. However, it should be noted that both of them used a higher working distance, more than 16 cm, than this present work, which settled at 5 cm. As such, it is likely the electrospinning jet was still in the early stage of the linear jet section, which would result in liquid fibers. Using higher working distance could help the drying of the electrospun fibers, however previous results have shown the detrimental effect of increasing working distance on 3D building with electrospinning [36]. The electric field simulations show all 3 base electrodes have the effect of straightening and uniformizing the electric field direction, which would further reduce the whipping motion of the electrospun jet [79,81,82].

The steering electrode was a floating ring placed mid-way of the electrospinning path, 2.5 cm from the collector, with no connection to the ground or external voltage applied. In previous research, rings electrodes were shown to reduce the whipping motion and thus narrow the deposition area [83]. At this relatively short distance, the ring is too close to the collector and act as a converging point for the electrospun fibers before getting into contact with the collector. As seen in Fig. 9, the controlled shaping of the 3D cylin-

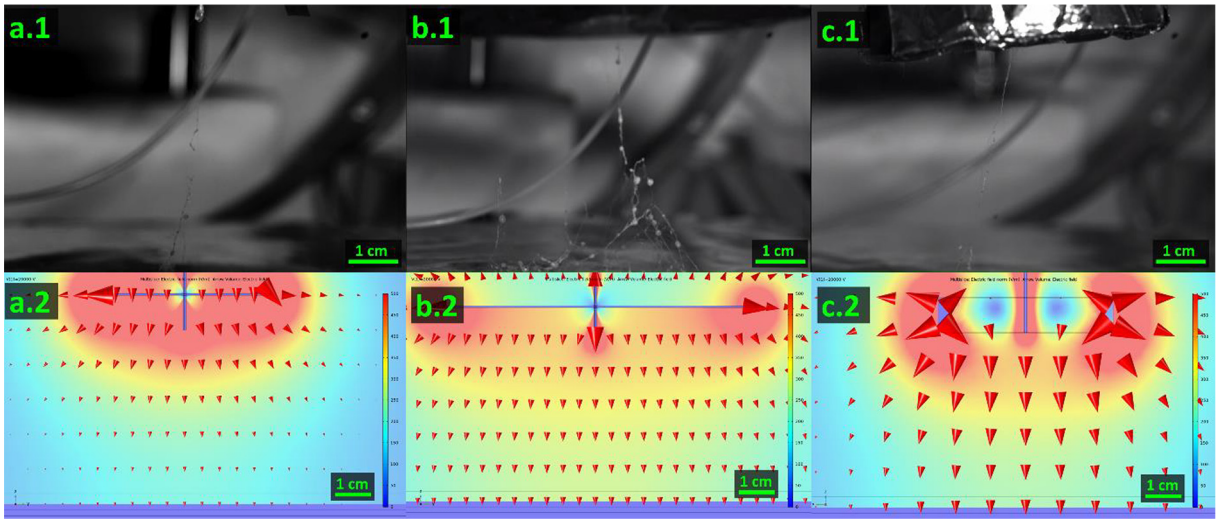

Fig. 8. Effect of base electrodes on 3D electrospinning. (a.1) High FPS camera photograph and (a.2) electric field simulations of electrospinning with a 5 cm aluminum foil circle base electrode, where (b.1) and (b.2) 10 cm aluminum foil circle and, (c.1) and (c.2) 5.5 cm aluminum ring. The base electrodes decrease the whipping motion of the electrospun jet, resulting in a wet line.

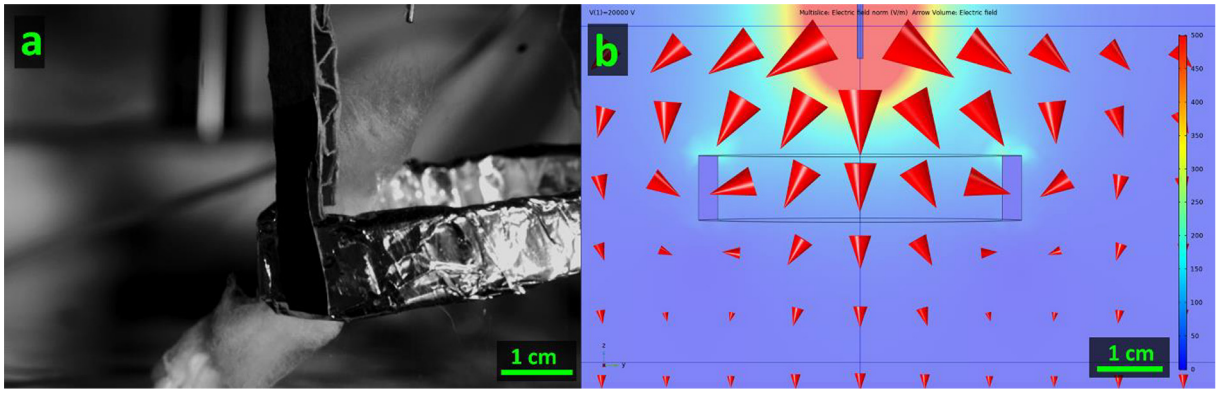

Fig. 9. Effect of steering electrodes on 3D electrospinning. (a) High FPS camera photograph and (b) Electric field simulation of electrospinning with a 5.5 cm aluminum ring electrode. As no voltage is applied to the ring, the electrospun jet can converge to it.

der is hindered by the steering ring, and the final 3D structure is a 3D bundle of fibers linking the ring and the collector, instead of the expected cylinder. The converging behavior induced by the ring is similar to that shown in previous research. It has been demonstrated that placing an electrode, grounded or charged, in close proximity to the collector's surface, results in the produced fibers being attracted towards the electrode [76,84]. The electric field simulation further confirms the tendency of the electrode ring to redirect the electric field lines [81]. Future work could assess the effect of adding a positive voltage to the ring to repel the jet and focus it onto the collector, as done in Salim A. et al's work [85]. However, based on our observations, as with the base electrode, this is most likely going to lead to a linear jet with poor drying due to the short working distance.

The guiding electrodes used were in the shapes of two parallel rectangles or a 5.5 cm ring, placed on the grounded collector. Although the guiding electrodes are not placed below the collector, they still act as guiding electrode as they modify the electric field in the vicinity of the collector and divert the deposition area toward a preferential site. The rectangles were used in an attempt to mimic the effect of parallel electrodes collector, as they can induce fibers alignment because the electric field lines are attracted towards the separated electrodes [77,86]. The 5.5 cm ring was shaped as the pattern of the nozzle head, which purpose was to act as an converging point similar to a tip guiding electrode [87]. The effect of both electrode configuration can be seen in Fig. 10. These grounded electrodes attract the electrospinning jet and influence the shape of the final 3D structure. A rectangle structure

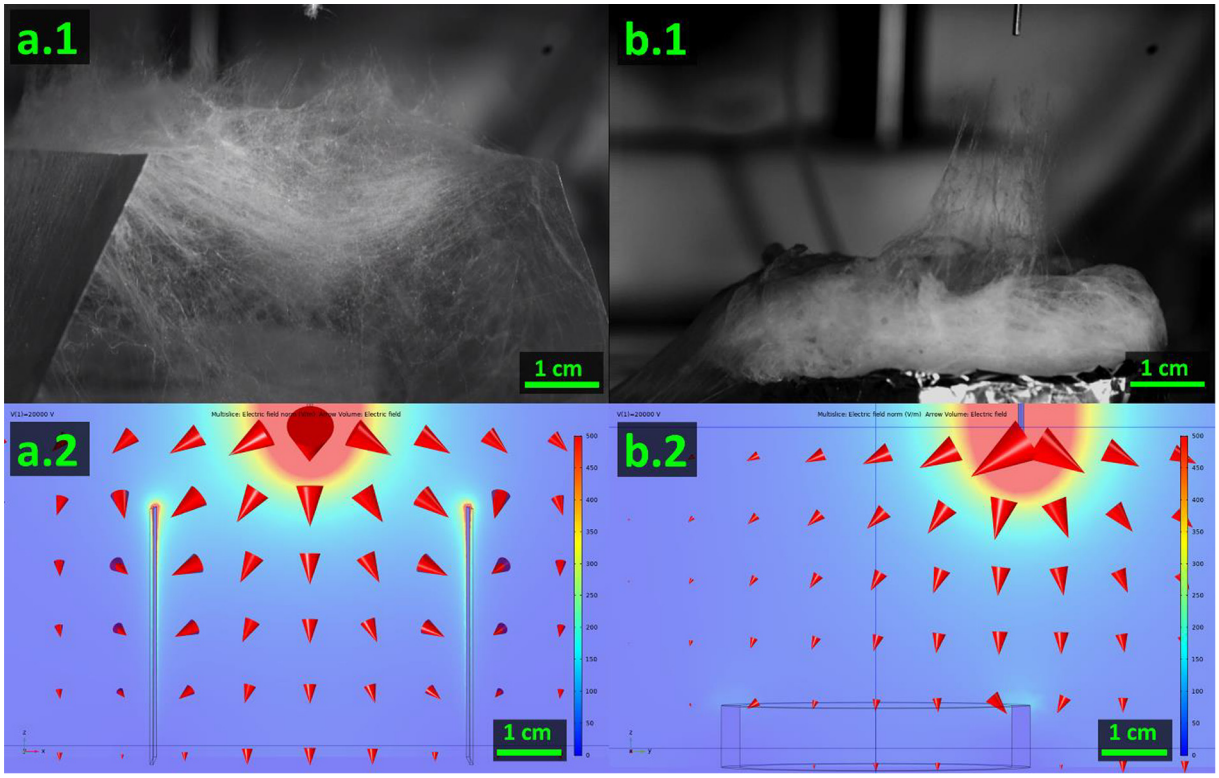

Fig. 10. Effect of guiding electrodes on 3D electrospinning. (a.1) High FPS camera photograph and (a.2) Electric field simulations of electrospinning with two parallel aluminum rectangles. (b.1) High FPS camera photograph and (b.2) Electric field simulations of electrospinning with a 5.5 cm aluminum ring put on the collector. The guiding electrodes help to shape the electrospun 3D structure.

is built up when using the parallel rectangles electrodes, despite using a circle nozzle pattern. The fibers are also unable to travel down to the grounded collector as the electrodes act as converging planes for the electrospun fibers. This behavior is explained with electric field simulations which highlight the electric field lines pointing toward the top of the rectangle electrode, no matter the position of the nozzle head. The 5.5 cm ring electrode has a more prominent effect on the 3D structure as it matches the movement of the nozzle head. The final electrospun structure is closer to the shape of a cylinder as it does not have a flat layer of fibers covering the collector. This is in contrast with previous works on self-assembly of electrospun fibres, where that initial flat layer is a necessary step to prevent the electrospun fibres from discharging through the ground, and thus, enable the 3D build-up [36,37]. Guiding electrodes can, in effect, accelerate the 3D build-up process and build 3D structures with higher shape fidelity. As confirmed by the electric field simulations in Fig. 10, the electrode ring diverts the electric field lines at the collector level. In effect, it focuses the incoming electrospun jet on the ring electrode and this help to shape the base of the cylinder as well as enhance the repulsion between fibers for 3D build-up. The effect of guiding electrodes is going in line with previous researches and simulations [77,88-90].

In an attempt to further investigate the control induced by a guiding electrode, the circle ring was replaced with a flower-shaped electrode of a similar size. The final 3D structure still had the shape of a cylinder, as it was following the pattern of the nozzle head, rather than the shape of the electrode itself. Photographs of the flower electrode and resulting 3D structures are shown in Figure S2.

The 5.5 cm ring guiding electrode was also used for electrospinning of 3D PAN and PVP in an attempt to help the electrospinning jet follow the designed shape. As there was no reduction in the whipping motion during electrospinning, no preferential shape in the final electrospun 3D structures of PAN and PVP was obtained, and the electrode was covered with fluffy polymer. There was no increase in the observed height of the obtained specimens either, as the additional height was only apparent due to the size of the ring electrode itself. Photographs of these 3D structures on the ring electrode are shown in Figure S3.

3.5. Scaling up

Further work has indicated that higher height structure can be obtained by increasing the working distance during electrospinning. This is similar to how the nozzle head has to be regularly lifted in an upward motion during precise near-field electrospinning to keep stacking layers of fibers on a 3D architecture [40]. Fig. 11 depicts a photograph of a tall 3D PS structure, built using the same experimental parameters than previously mentioned but by steadily increasing the working distance by 1 cm every 2 min. Starting from a working distance of 5 cm, a final working distance of 10 cm was set after 10 min of 3D electrospinning. This taller 3D PS structure has a height of 5.0 ± 0.1 cm, making it 60% taller than the original one. However, it boasts an average wall thickness of 2.6 ± 0.1 cm, which is 0.2 cm thicker than the original 3D structure. More fibers are also present around the 3D structure. This small loss in resolution is due to the wider whipping motion occurring at a higher working distance as the 3D structure itself is not as attractive as the grounded collector [36]. Our previous study has shown that 3D electrospinning from an initial working distance of 10 cm would cause the electrospun fibres to be spread in the whole electrospinning chamber, this is because of the relative attraction of the nozzle collecting belt. This incremental vertical movement allows for a slow and guided deposition of the electrospun fibres on top of the 3D structure, which enables the fabrication of 3D structures taller than previously reported [36].

Electrospinning with a dynamic distance up to 20 cm was also attempted. However, the electrospun jet would no longer be attracted to the structure on the collector past a working distance of 10 cm. This is because of the weaker electric field at higher working distance, as explained in previous research [91,92]. Overall, the 3D structure loses the shape of the designed cylinder and crumbles down in a fashion similar to Sun B. et al's 3D structures electrospun at a working distance of 15 cm [37]. Photographs of the collapsed 3D structure are shown in Figure S4.

The electrospinning of designed 3D structures for PS, PVP and PAN polymers has been shown using a custom 3D electrospinning device, as discussed previously. In an attempt to show the versatility of the 3D electrospinning process, a conventional electrospinning device and a nozzle-free electrospinning setup were assessed with the optimized PS, PAN and PVP solutions. A low degree of 3D build-up was observed in both setups, with noticeable drawbacks compared to the 3D electrospinning device. For conventional electrospinning, as the nozzle is staying immobile, the path of the electrospun jet is focused on a smaller area. This leads to faster initial build-up, but less stretching of the fibers and more instability of the jet as the 3D structure gets closer to the nozzle head. When the 3D structure gets too close to the nozzle head, the outcoming electrospun fibers can get stuck to the nozzle, which in turn renders the electrospinning process unstable. In the case of PS, in Figure S5, the whipping motion of the electrospun fibers is lessened. This hinders the evaporation of the organic solvent and results in the deposition of wet polymer on the collector. For 3D

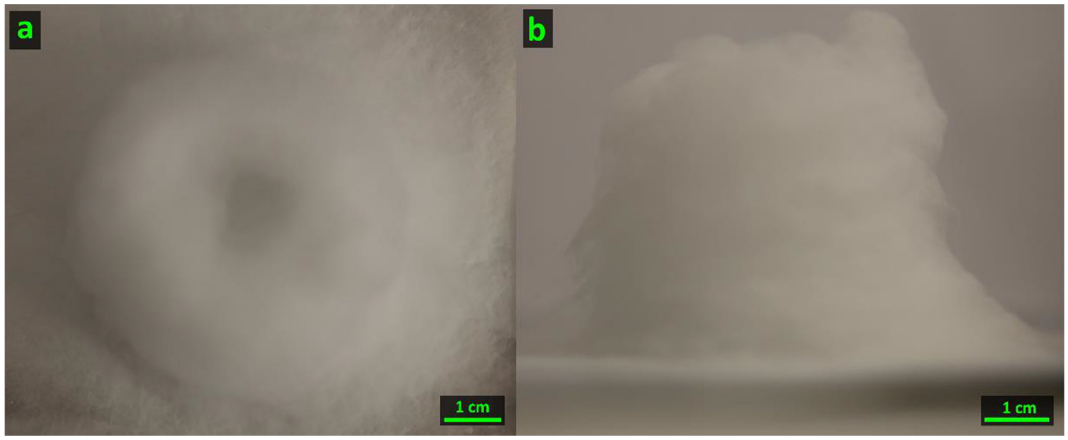

Fig. 11. 3D PS structure electrospun with increasing working distance, the final structure is taller. (a) Top-view of the 3D structure. (b) Side-view of the 3D structure.

PAN and 3D PVP, dripping of the polymer solution occurs which partially dissolves the electrospun structure. All polymers also show high beads content after electrospinning in these conditions as seen in the SEM pictures. To resolve the instability problem, it is necessary to lower the flow rate to decrease the build-up speed of the 3D structure and prevent wet fibers and beads. In general, a flow rate too high can result in the formation of beads, non-uniform fibers, secondary fiber morphologies (*e.g.* spider nets), droplets and wet fiber-deposition due to the larger initial electrospinning jet and decreased whipping motion [47,93-95]. This observation is true for all three polymers and the flowrate has to be tuned from 5 $mL.h^{-1}$ to 3 $mL.h^{-1}$ for PVP and down to 1 $mL.h^{-1}$ for PS and PAN. The direct consequence of this adjustment is the lower production rate, going from the optimized ~ 750 ± 10 $mg.h^{-1}$ to ~ 160 ± 4 $mg.h^{-1}$ and from ~ 338 ± 10 $mg.h^{-1}$ to ~ 218 ± 7 $mg.h^{-1}$ for PS and PAN respectively. The fibers diameter is also reduced with a lower flowrate, going from 0.85 ± 0.02 μm to 0.54 ± 0.01 μm, from 0.74 ± 0.01 μm to 0.65 ± 0.01 μm and from 1.04 ± 0.02 μm to 0.66 ± 0.01 μm for PS, PAN and PVP, respectively. This decreasing trend goes in line with previous studies [47,96,97]. The photographs and SEM micrographs of the 3D structures electrospun with a single-needle setup are shown in Fig. 12. The PS structure has the shape of a pillar, 4.4 ± 0.1 cm in height and 1.4 ± 0.1 cm in average thickness. The PAN and PVP structures both have the shape of a cone, PAN with a height of 2.1 ± 0.1 cm, a base thickness of 8.5 ± 0.1 cm and a top thickness of 3.1 ± 0.1 cm, and PVP with a height of 1.7 ± 0.1 cm, a base thickness of 2.8 ± 0.1 cm and a top thickness of 0.7 ± 0.1 cm. The dimensions of the 3D structures obtained using the conventional electrospinning setup are, in all cases, smaller than the ones electrospun with the 3D electrospinning technique, as shown in Fig. 3.

With a nozzle-free electrospinning setup, 3D build-up was observed only for low collector rotation speed. The current setup allows for steady speed as low as 30 RPM. At this speed, only specific areas in the rotating collector's surface can achieve a 3D build-up and the overall height of the produced 3D structure is relatively short, being lower than 1 cm compared to the 4 cm obtained using the 3D electrospinning method. With a non-rotating drum, the 3D build-up is more uniform and covers the central area of the drum. By moving the deposition area of the drum every two minutes, it is possible to electrospin the 3D structure all around the drum and build a thick electrospun cylinder. For both PS and PAN, as seen in Fig. 13, the maximum height of the 3D structure is about 2.5 cm. The reason why the highest 3D build-up is achieved with a non-rotating drum could be related to the additional mechanical forces induced by a rotating cylinder. Previous studies have shown these forces pull the fibers towards the cylinder [98-100]. In hindsight, this is similar to how using a high-rotating speed drum collector favors the alignment of the electrospun fibers. The most widely accepted explanation to this phenomenon is that the high

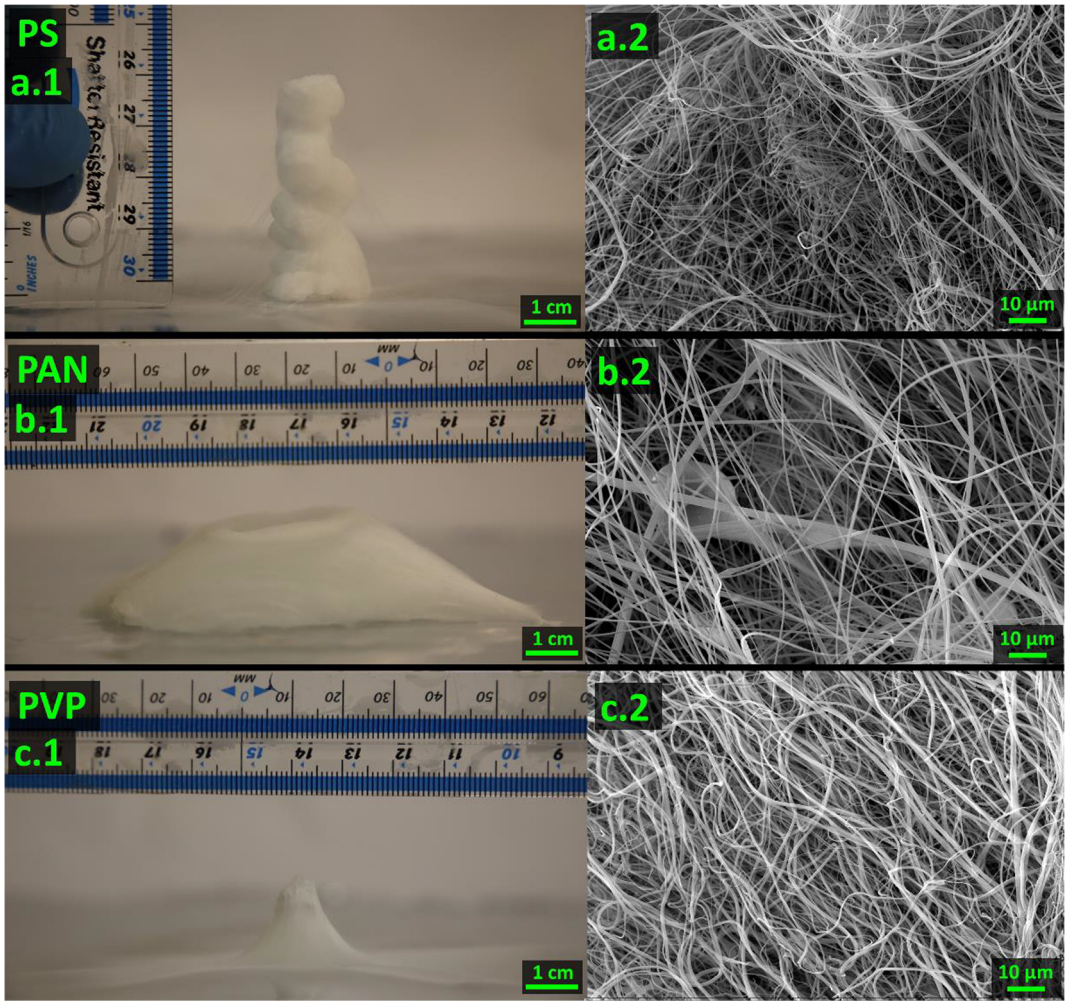

Fig. 12. 3D structures obtained using the single-needle electrospinning setup. Where (a.1) Photograph and (a.2) SEM of 3D PS structures, (b.1) photograph and (b.2) SEM of 3D PAN, and (c.1) photograph and (c.2) SEM of 3D PVP.

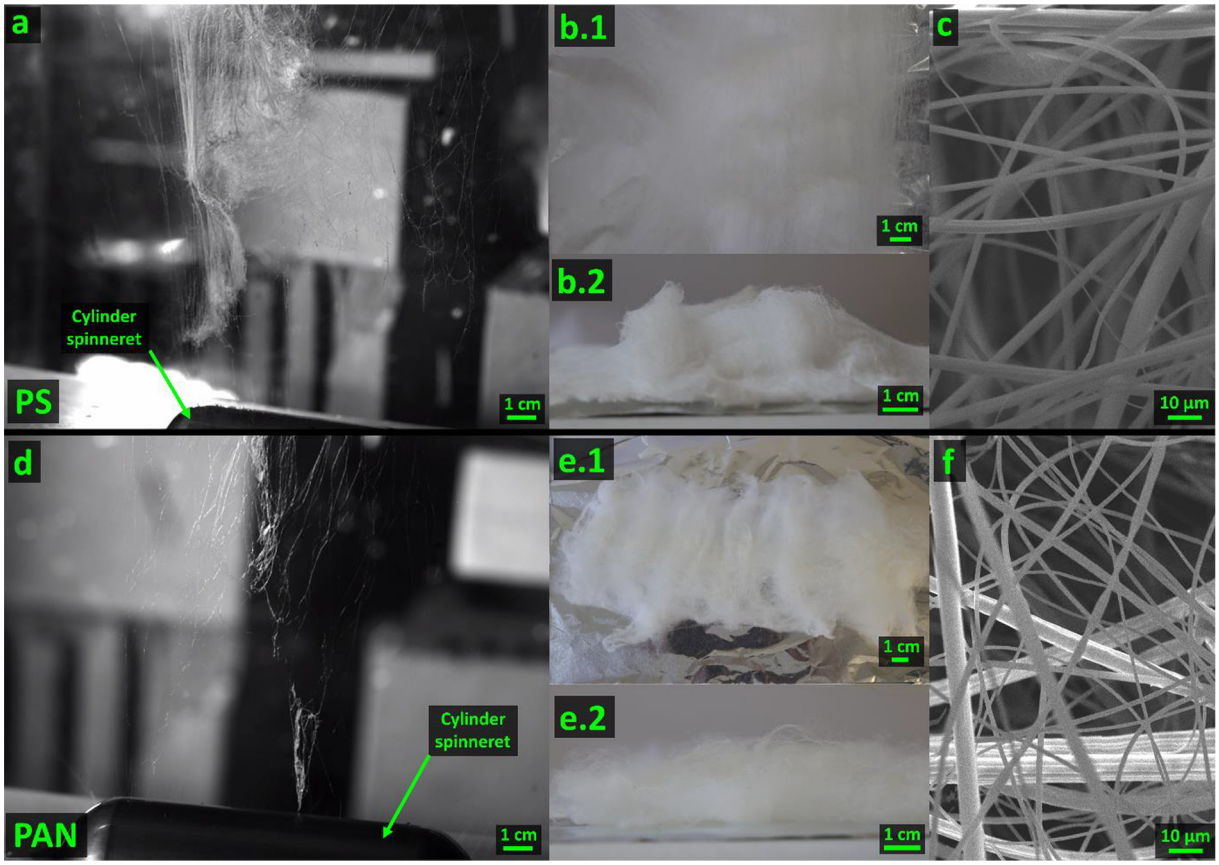

Fig. 13. 3D structures obtained using the nozzle-free electrospinning device. Where, (a) High FPS camera photograph, (b.1) and (b.2) Photograph and c) SEM pictures of 3D PS. (d), (e.1), (e.2) and (f) are photographs of the 3D PAN structures.

rotating speed of the drum causes additional drawing and stretching of the fibers [101-103]. Preventing rotation of the collecting drum would thus minimize the forces subjected to the electrospun fibers. The fibers diameter size ranged between 3.62 ± 0.14 µm and 2.45 ± 0.09 µm for PS and PAN, respectively, which is larger than the 3D structures produced using the single-needle setup. Using a rotating drum can yield bigger fibers diameter and wider size distribution. This is due to the non-desirable evaporation of the solvent in the bath, which leads to higher solution viscosity and thus increasing the diameter of the electrospun fibers [104,105]. Electrospinning of PVP using the needleless setup was not feasible for a similar reason. The high open surface of the setup favors evaporation of the PVP/MeOH solution before stable formation of the Taylor cones.

A major drawback of these two devices, when used to develop 3D configurations, is their poor control over the shape of the electrospun 3D structure as they lack the ability to move in a controlled pattern the deposition area of the electrospun fibers.

4. Conclusion

Electrospinning of 3D structures made of PS, PAN and PVP was achieved within 10 min in a single step. The height of the 3D structures ranged between 1 and 4 cm. All electrospun 3D structures exhibit long shelf-life; however, only the PS structures have good shape recovery against compression. This is because of the charge retention of the PAN fibers, which makes them attractive to the weight and skew the compression test, and the adhesive properties of PVP. While several acids and bases can be used to initiate the 3D build-up, it is still difficult to quantitatively explain the formation mechanism of the 3D structure. This study does go in-depth with several factors that could have induced the 3D build-up. There was no significant change of solution viscosity before and after the insertion of the additive causing the 3D build-up. Likewise, no strong interactions between the polymer and the additive were identified. No additional crystal phases were detected in the 3D polymer structure. Finally, while there is a substantial increase of conductivity after adding the acid or base additive, it is not directly related to the 3D build-up during electrospinning. Fully understanding the 3D build-up mechanism of 3D electrospinning could help to shape the final structure. For now, electrodes were used to steer the electrospinning jet or control the deposition area. Only guiding electrodes can mold the electrospun 3D structure. Base and steering electrodes hinder the whipping motion of the electrospun jet and lead to poor drying. While most of these studies were conducted using a custom 3D electrospinning device, it was shown that it is possible to obtain 3D build-up by using standard electrospinning and a nozzle-free electrospinning setup, at the cost of lacking the precise shaping of the 3D structures. This does, however, open up the possibility of manufacturing 3D electrospun structures on a commercial scale. 3D structures have promising applications in oil adsorption, energy storage or bioengineering as scaffolds for cell culture. In the future, more shapes of guiding electrodes should be used to further enhance the shaping of the 3D electrospun structures. It could be interesting to minimize as much as possible the wall resolution of 3D electrospinning. Another option would be to tune the temperature and humidity of the electrospinning chamber, to force a faster evaporation of the electrospun jet and solidification of the polymer. With fast solidification, it might be possible to draw 3D structures in a similar fashion to melt electrospinning.

Declaration of Competing Interest

The authors declare that they have no known competing financial interests or personal relationships that could have appeared to influence the work reported in this paper.

Acknowledgement

The authors would like to thank Dr. Richard Anthony Black and the UK Engineering & Physical Sciences Research Council (Grant ref. EP/K011952/1) for providing the high-speed camera. Special thanks are given to the Armourers and Brasiers' Gauntlet Trust for funding the oral presentation, which featured part of this research paper, that took place at the Electrospin2019 conference. Furthermore, we would like to recognize the Castansa Trust for their donation of the SEM (JEOL JSM-IT100) to the Radacsi research group.

Data availability

The raw/processed data required to reproduce these findings cannot be shared at this time due to technical or time limitations.

Appendix A. Supplementary material

Supplementary data to this article can be found online at https://doi.org/10.1016/j.matdes.2021.109916.

References

[1] A. El-hadi, F. Al-Jabri, Influence of Electrospinning Parameters on Fiber Diameter and Mechanical Properties of Poly(3-Hydroxybutyrate) (PHB) and Polyanilines (PANI) Blends, Polymers (Basel). 8 (2016) 97.
[2] V. Beachley, X. Wen, Effect of electrospinning parameters on the nanofiber diameter and length, Mater. Sci. Eng. C 29 (2009) 663–668.
[3] V. Milleret, T. Hefti, H. Hall, V. Vogel, D. Eberli, Influence of the fiber diameter and surface roughness of electrospun vascular grafts on blood activation, Acta Biomater. 8 (2012) 4349–4356.
[4] F.J. García-Mateos, R. Ruiz-Rosas, J.M. Rosas, J. Rodríguez-Mirasol, T. Cordero, Controlling the composition, morphology, porosity, and surface chemistry of lignin-based electrospun carbon materials, Front. Mater. 6 (2019) 1–16.
[5] J. Rnjak-Kovacina, A.S. Weiss, Increasing the Pore Size of Electrospun Scaffolds, Tissue Eng. Part B Rev. 17 (2011) 365–372.
[6] H. Yuan, Q. Zhou, Y. Zhang, Improving fiber alignment during electrospinning, in: Electrospun Nanofibers, Elsevier, 2017. Pp. 125–147. doi:10.1016/B978-0-08-100907-9.00006-4.
[7] Y. Liu, J.-H. He, J. Yu, H. Zeng, Controlling numbers and sizes of beads in electrospun nanofibers, Polym. Int. 57 (2008) 632–636.
[8] S. Homaeigohar, Y. Davoudpour, Y. Habibi, M. Elbahri, The Electrospun Ceramic Hollow Nanofibers, Nanomaterials 7 (2017) 383.
[9] Z.-X. Huang, J.-W. Wu, S.-C. Wong, J.-P. Qu, T.S. Srivatsan, The technique of electrospinning for manufacturing core-shell nanofibers, Mater. Manuf. Process. 33 (2018) 202–219.
[10] K. Tang, Y. Yu, X. Mu, P.A. Van Aken, J. Maier, Multichannel hollow TiO2 nanofibers fabricated by single-nozzle electrospinning and their application for fast lithium storage, Electrochem. commun. 28 (2013) 54–57.
[11] Y. Li, J. Gong, Y. Deng, Hierarchical structured ZnO nanorods on ZnO nanofibers and their photoresponse to UV and visible lights, Sensors Actuators, A Phys. 158 (2010) 176–182.
[12] R. Faridi-Majidi, M. Madani, N. Sharifi-Sanjani, S. Khoee, A. Fotouhi, Multi-Phase Composite Nanofibers via Electrospinning of Latex Containing Nanocapsules with Core-Shell Morphology, Polym. Plast. Technol. Eng. 51 (2012) 364–368.
[13] H. Chen et al., Nanowire-in-Microtube Structured Core/Shell Fibers via Multifluidic Coaxial Electrospinning, Langmuir 26 (2010) 11291–11296.
[14] H. Wu, R. Zhang, X. Liu, D. Lin, W. Pan, Electrospinning of Fe Co, and Ni Nanofibers: Synthesis, Assembly, and Magnetic Properties, Chem. Mater. 19 (2007) 3506–3511.
[15] J. Geltmeyer et al., The influence of tetraethoxysilane sol preparation on the electrospinning of silica nanofibers, J. Sol-Gel Sci. Technol. 77 (2016) 453–462.
[16] S. Lee, B. Kim, S.-H. Kim, E. Kim, J.-H. Jang, Superhydrophobic, Reversibly Elastic, Moldable, and Electrospun (SupREME) Fibers with Multimodal Functions: From Oil Absorbents to Local Drug Delivery Adjuvants, Adv. Funct. Mater. 27 (2017) 1702310.
[17] Y. Huang et al., Elastic Carbon Aerogels Reconstructed from Electrospun Nanofibers and Graphene as Three-Dimensional Networked Matrix for Efficient Energy Storage/Conversion, Sci. Rep. 6 (2016) 31541.
[18] Y. Si, J. Yu, X. Tang, J. Ge, B. Ding, Ultralight nanofibre-assembled cellular aerogels with superelasticity and multifunctionality, Nat. Commun. 5 (2014) 5802.
[19] Y.-Z. Lin et al., Facile synthesis of electrospun carbon nanofiber/graphene oxide composite aerogels for high efficiency oils absorption, Environ. Int. 128 (2019) 37–45.
[20] D. Kołbuk, M. Heljak, E. Choińska, O. Urbanek, Novel 3D Hybrid Nanofiber Scaffolds for Bone Regeneration, Polymers (Basel) 12 (2020) 544.
[21] L.F. Mellor et al., Fabrication and Evaluation of Electrospun, 3D-Bioplotted, and Combination of Electrospun/3D-Bioplotted Scaffolds for Tissue Engineering Applications, Biomed Res. Int. 2017 (2017) 1–9.
[22] X. Jing, H. Li, H.-Y. Mi, Y.-J. Liu, Y.-M. Tan, Fabrication of fluffy shish-kebab structured nanofibers by electrospinning, CO2 escaping foaming and controlled crystallization for biomimetic tissue engineering scaffolds, Chem. Eng. J. 372 (2019) 785–795.
[23] J.I. Kim, J.Y. Kim, C.H. Park, Fabrication of transparent hemispherical 3D nanofibrous scaffolds with radially aligned patterns via a novel electrospinning method, Sci. Rep. 8 (2018) 3424.
[24] H. Sun et al., Hierarchical 3D electrodes for electrochemical energy storage, Nat. Rev. Mater. 4 (2019) 45–60.
[25] Z. Wang et al., Freestanding nanocellulose-composite fibre reinforced 3D polypyrrole electrodes for energy storage applications, Nanoscale 6 (2014) 13068–13075.
[26] S. Wang et al., Flexible MoO 2 Nanocrystals@N-doped Carbon Nanofibers Film as a Self-Supporting Anode for Quasi-Solid-State Sodium-Ion Batteries, Energy Technol. 9 (2021) 2000820.
[27] W. Zhang et al., Efficient electrospinning fabrication and the underlying formation mechanism of one-dimensional monoclinic Li 2 FeSiO 4 nanofibers, CrystEngComm 21 (2019) 6340–6345.
[28] Y. Chen, M. Shafiq, M. Liu, Y. Morsi, X. Mo, Advanced fabrication for electrospun three-dimensional nanofiber aerogels and scaffolds, Bioact. Mater. 5 (2020) 963–979.
[29] B. Sun et al., Advances in three-dimensional nanofibrous macrostructures via electrospinning, Prog. Polym. Sci. 39 (2014) 862–890.
[30] N. Shah Hosseini et al., Novel 3D electrospun polyamide scaffolds prepared by 3D printed collectors and their interaction with chondrocytes, Int. J. Polym. Mater. Polym. Biomater. 67 (2018) 143–150.
[31] G. Duan et al., Ultralight, Soft Polymer Sponges by Self-Assembly of Short Electrospun Fibers in Colloidal Dispersions, Adv. Funct. Mater. 25 (2015) 2850–2856.
[32] M.K. Joshi et al., Multi-layered macroporous three-dimensional nanofibrous scaffold via a novel gas foaming technique, Chem. Eng. J. 275 (2015) 79–88.
[33] L. Cao, Y. Si, X. Yin, J. Yu, B. Ding, Ultralight and Resilient Electrospun Fiber Sponge with a Lamellar Corrugated Microstructure for Effective Low-Frequency Sound Absorption, ACS Appl. Mater. Interfaces 11 (2019) 35333–35342.
[34] M.M. Li, Y.Z. Long, Fabrication of Self-Assembled Three-Dimensional Fibrous Stackings by Electrospinning, Mater. Sci. Forum 688 (2011) 95–101.
[35] M. Cheng, Z. Qin, S. Hu, H. Yu, M. Zhu, Use of electrospinning to directly fabricate three-dimensional nanofiber stacks of cellulose acetate under high relative humidity condition, Cellulose 24 (2017) 219–229.
[36] M. Vong et al., Controlled three-dimensional polystyrene micro- and nano-structures fabricated by three-dimensional electrospinning, RSC Adv. 8 (2018) 15501–15512.
[37] B. Sun et al., Self-assembly of a three-dimensional fibrous polymer sponge by electrospinning, Nanoscale 4 (2012) 2134.
[38] F.M. Wunner et al., Melt Electrospinning Writing of Highly Ordered Large Volume Scaffold Architectures, Adv. Mater. 30 (2018) 1706570.
[39] T.D. Brown, P.D. Dalton, D.W. Hutmacher, Direct Writing By Way of Melt Electrospinning, Adv. Mater. 23 (2011) 5651–5657.
[40] G. Luo et al., Direct-Write, Self-Aligned Electrospinning on Paper for Controllable Fabrication of Three-Dimensional Structures, ACS Appl. Mater. Interfaces 7 (2015) 27765–27770.
[41] H.G. Lemu, Study of capabilities and limitations of 3D printing technology, AIP Conf. Proc. 1431 (2012) 857–865.
[42] Y. Zheng, N. Meng, B. Xin, Effects of Jet Path on Electrospun Polystyrene Fibers, Polymers (Basel) 10 (2018) 842.
[43] C.-M. Wu, H.-G. Chiou, S.-L. Lin, J.-M. Lin, Effects of electrostatic polarity and the types of electrical charging on electrospinning behavior, J. Appl. Polym. Sci. 126 (2012) E89–E97.
[44] A.A. Lach et al., Pyridine as an additive to improve the deposition of continuous electrospun filaments, PLoS ONE 14 (2019) e0214419.
[45] A. Haider, S. Haider, I.-K. Kang, A comprehensive review summarizing the effect of electrospinning parameters and potential applications of nanofibers in biomedical and biotechnology, Arab. J. Chem. 11 (2018) 1165–1188.
[46] S.A. Theron, E. Zussman, A.L. Yarin, Experimental investigation of the governing parameters in the electrospinning of polymer solutions, Polymer (Guildf). 45 (2004) 2017–2030.
[47] S. Zargham, S. Bazgir, A. Tavakoli, A.S. Rashidi, R. Damerchely, The Effect of Flow Rate on Morphology and Deposition Area of Electrospun Nylon 6 Nanofiber, J. Eng. Fiber. Fabr. 7 (2012). 155892501200700.

[48] M.Y. Kariduraganavar, A.A. Kittur, R. R. Kamble, Polymer Synthesis and Processing. in Natural and Synthetic Biomedical Polymers 1–31, Elsevier, 2014. doi:10.1016/B978-0-12-396983-5.00001-6.
[49] S. Fitzpatrick, J.F. McCabe, C.R. Petts, S.W. Booth, Effect of moisture on polyvinylpyrrolidone in accelerated stability testing, Int. J. Pharm. 246 (2002) 143–151.
[50] Y.Z. Beju, J.N. Mandal, Compression creep test on expanded polystyrene (EPS) geofoam, Int. J. Geotech. Eng. 10 (2016) 401–408.
[51] R.P.K. Jeya, A.H. Bouzid, Compression Creep and Thermal Ratcheting Behavior of High Density Polyethylene (HDPE), Polymers (Basel) 10 (2018) 156.
[52] S. Lee et al., Highly Moldable Electrospun Clay-Like Fluffy Nanofibers for Three-Dimensional Scaffolds, ACS Appl. Mater. Interfaces 6 (2014) 1082–1091.
[53] H.L. Schreuder-Gibson, P. Gibson, P. Tsai, Cooperative Charging Effects of Fibers from Electrospinning of Electrically Dissimilar Polymers. Int. Nonwovens J. os-13 (2004) 1558925004os–13.
[54] M. Teodorescu, M. Bercea, Poly(vinylpyrrolidone) – A Versatile Polymer for Biomedical and Beyond Medical Applications, Polym. Plast. Technol. Eng. 54 (2015) 923–943.
[55] J. Lee, Intrinsic Adhesion Properties of Poly(vinyl pyrrolidone) to Pharmaceutical Materials: Humidity Effect, Macromol. Biosci. 5 (2005) 1085–1093.
[56] T. Uyar, F. Besenbacher, Electrospinning of uniform polystyrene fibers: The effect of solvent conductivity, Polymer (Guildf). 49 (2008) 5336–5343.
[57] Z. Khan et al., Morphology, Mechanical Properties and Surface Characteristics of Electrospun Polyacrylonitrile (PAN) Nanofiber Mats, Int. J. Adv. Eng. Nano Technol. 2 (2015) 15–22.
[58] S. Chuangchote, T. Sagawa, S. Yoshikawa, Electrospinning of poly(vinyl pyrrolidone): Effects of solvents on electrospinnability for the fabrication of poly(p -phenylene vinylene) and TiO 2 nanofibers, J. Appl. Polym. Sci. 114 (2009) 2777–2791.
[59] C.Y. Liang, S. Krimm, Infrared spectra of high polymers, VI. Polystyrene. *J. Polym. Sci.* 27 (1958) 241–254.
[60] G. Chen, S. Liu, S. Chen, Z. Qi, FTIR spectra, thermal properties, and dispersibility of a polysterene/montmorillonite nanocomposite, Macromol. Chem. Phys. 202 (2001) 1189–1193.
[61] A. Imhof, Preparation and characterization of titania-coated polystyrene spheres and hollow titania shells, Langmuir 17 (2002) 3579–3585.
[62] C. Huang et al., Needleless Electrospinning of Polystyrene Fibers with an Oriented Surface Line Texture, J. Nanomater. 2012 (2012) 1–7.
[63] J. Fang, Y. Xuan, Q. Li, Preparation of polystyrene spheres in different particle sizes and assembly of the PS colloidal crystals, Sci. China Technol. Sci. 53 (2010) 3088–3093.
[64] D. Wankasi, E.D. Dikio, Comparative Study of Polystyrene and Polymethylmethacrylate Wastes as Adsorbents for Sorption of Pb2+ from Aqueous Solution, Asian J. Chem. 26 (2014) 8295–8302.
[65] S. Huan, L. Bai, G. Liu, W. Cheng, G. Han, Electrospun nanofibrous composites of polystyrene and cellulose nanocrystals: manufacture and characterization, RSC Adv. 5 (2015) 50756–50766.
[66] Meireles, C. da S., Filho, G. R., de Assunção, R. M. N., Zeni, M. & Mello, K. Blend compatibility of waste materials—Cellulose acetate (from sugarcane bagasse) with polystyrene (from plastic cups): Diffusion of water, FTIR, DSC, TGA, and SEM study. J. Appl. Polym. Sci. 104 (2007) 909–914.
[67] O.J. Rojas, G.A. Montero, Y. Habibi, Electrospun nanocomposites from polystyrene loaded with cellulose nanowhiskers, J. Appl. Polym. Sci. 113 (2009) 927–935.
[68] J.E.K. Schawe, Vitrification in a wide cooling rate range: The relations between cooling rate, relaxation time, transition width, and fragility, J. Chem. Phys. 141 (2014) 184905.
[69] M.L. Arnal, A.J. Müller, P. Maiti, M. Hikosaka, Nucleation and crystallization of isotactic poly(propylene) droplets in an immiscible polystyrene matrix, Macromol. Chem. Phys. 201 (2000) 2493–2504.
[70] C.A. Bonino et al., Three-Dimensional Electrospun Alginate Nanofiber Mats via Tailored Charge Repulsions, Small 8 (2012) 1928–1936.
[71] H.-Y. Mi, X. Jing, H.-X. Huang, L.-S. Turng, Instantaneous self-assembly of three-dimensional silica fibers in electrospinning: Insights into fiber deposition behavior, Mater. Lett. 204 (2017) 45–48.
[72] A. Weissberger, J.A. Riddick, W.B. Bunger, T.K. Sakano, Organic Solvents, Fourth Edition (Techniques of Chemistry, Volume 2). vol. 2 (1986).
[73] R.C. Weast, Handbook of Chemistry and Physics, 68th Edition. CRC Press, 1987.
[74] M. Yousefzadeh, M. Latifi, M. Amani-Tehran, W.-E. Teo, S. Ramakrishna, A Note on the 3D Structural Design of Electrospun Nanofibers. J. Eng. Fiber. Fabr. 7 (2012) 155892501200700.
[75] W.-E. Teo, R. Inai, S. Ramakrishna, Technological advances in electrospinning of nanofibers, Sci. Technol. Adv. Mater. 12 (2011) 013002.
[76] M. Yousefzadeh, S. Ramakrishna, Modeling performance of electrospun nanofibers and nanofibrous assemblies, in: Electrospun Nanofibers, Elsevier, 2017, 303–337. doi:10.1016/B978-0-08-100907-9.00013-1.
[77] K. Oncheurn, Y. Infahsaeng, Electric field effect on electrospun fiber alignment using a parallel electrode plate, J. Phys. Conf. Ser. 1719 (2021) 012064.
[78] L. Buttafoco et al., Electrospinning of collagen and elastin for tissue engineering applications, Biomaterials 27 (2006) 724–734.
[79] Y. Yang et al., Effect of electric field distribution uniformity on electrospinning, J. Appl. Phys. 103 (2008) 104307.
[80] N.N. Bunyan, J. Chen, I. Chen, S. Farboodmanesh, Electrostatic Effects on Electrospun Fiber Deposition and Alignment, ACS Symp. Ser. 918 (2006) 106–120.
[81] K. Smółka, A. Firych-Nowacka, M. Lefik, Three-dimensional computer models of electrospinning systems, Open Phys. 15 (2017) 777–789.
[82] R. Sahay, V. Thavasi, S. Ramakrishna, Design Modifications in Electrospinning Setup for Advanced Applications, J. Nanomater. 2011 (2011) 1–17.
[83] J.M. Deitzel, J.D. Kleinmeyer, J.K. Hirvonene, N.C., B. T. Controlled deposition of electrospun poly(ethylene oxide) fibers. Polymer (Guildf). 42 (2001) 8163–8170.
[84] G. Kim, W. Kim, Nanofiber spraying method using a supplementary electrode, Appl. Phys. Lett. 89 (2006) 013111.
[85] A. Salim, C. Son, B. Ziaie, Selective nanofiber deposition via electrodynamic focusing, Nanotechnology 19 (2008) 375303.
[86] C. Fryer, M. Scharnagl, C. Helms, Electrostatic alignment of electrospun PEO fibers by the gap method increases individual fiber modulus in comparison to non-aligned fibers of similar diameter, AIP Adv. 8 (2018) 065023.
[87] G. Zheng et al., High-aspect-ratio three-dimensional electrospinning via a tip guiding electrode, Mater. Des. 198 (2021) 109304.
[88] M. Vong, N. Radacsi, Fabrication of radially aligned electrospun nanofibers in a three-dimensional conical shape, Electrospinning 2 (2018) 1–14.
[89] D. Li, Y. Wang, Y. Xia, Electrospinning of polymeric and ceramic nanofibers as uniaxially aligned arrays, Nano Lett. 3 (2003) 1167–1171.
[90] A. Theron, E. Zussman, A.L. Yarin, Electrostatic field-assisted alignment of electrospun nanofibres, Nanotechnology 12 (2001) 384–390.
[91] B. Robb, & B. Lennox, The electrospinning process, conditions and control, in: Electrospinning for Tissue Regeneration, Elsevier, 2011, 51–66. doi:10.1533/9780857092915.1.51.
[92] S. Jin, B. Xin, Y. Zheng, S. Liu, Effect of Electric Field on the Directly Electrospun Nanofiber Yarns: Simulation and Experimental Study, Fibers Polym. 19 (2018) 116–124.
[93] C. Zhang, X. Yuan, L. Wu, Y. Han, J. Sheng, Study on morphology of electrospun poly(vinyl alcohol) mats, Eur. Polym. J. 41 (2005) 423–432.
[94] M. Chowdhury, G. Stylios, Effect of experimental parameters on the morphology of electrospun Nylon 6 fibres, Int. J. Basic Appl. Sci. 10 (2010) 70–78.
[95] S.-H. Chen, Y. Chang, K.-R. Lee, J.-Y. Lai, A three-dimensional dual-layer nano/microfibrous structure of electrospun chitosan/poly(d, l-lactide) membrane for the improvement of cytocompatibility, J. Memb. Sci. 450 (2014) 224–234.
[96] V. Milleret, B. Simona, P. Neuenschwander, H. Hall, Tuning electrospinning parameters for production of 3D-fiber-fleeces with increased porosity for soft tissue engineering applications, Eur. Cells Mater. 21 (2011) 286–303.
[97] C. Wang et al., Correlation between processing parameters and microstructure of electrospun poly(D, l-lactic acid) nanofibers, Polymer (Guildf). 50 (2009) 6100–6110.
[98] M.D. Edwards, G.R. Mitchell, S.D. Mohan, R.H. Olley, Development of orientation during electrospinning of fibres of poly(ε-caprolactone), Eur. Polym. J. 46 (2010) 1175–1183.
[99] L. Yu, Z. Shao, L. Xu, M. Wang, High Throughput Preparation of Aligned Nanofibers Using an Improved Bubble-Electrospinning, Polymers (Basel) 9 (2017) 658.
[100] S. Haider et al., Highly aligned narrow diameter chitosan electrospun nanofibers, J. Polym. Res. 20 (2013) 105.
[101] Z.-M. Huang, Y.-Z. Zhang, M. Kotaki, S. Ramakrishna, A review on polymer nanofibers by electrospinning and their applications in nanocomposites, Compos. Sci. Technol. 63 (2003) 2223–2253.
[102] A. Baji, Y.-W. Mai, S.-C. Wong, M. Abtahi, P. Chen, Electrospinning of polymer nanofibers: Effects on oriented morphology, structures and tensile properties, Compos. Sci. Technol. 70 (2010) 703–718.
[103] S.F. Fennessey, R.J. Farris, Fabrication of aligned and molecularly oriented electrospun polyacrylonitrile nanofibers and the mechanical behavior of their twisted yarns, Polymer (Guildf). 45 (2004) 4217–4225.
[104] G. Yan, H. Niu, T. Lin, Needle-less Electrospinning, in: Electrospinning: Nanofabrication and Applications, vol. 2, Elsevier, 2019, pp. 219–247.
[105] F. Yener, O. Jirsak, Comparison between the Needle and Roller Electrospinning of Polyvinylbutyral, J. Nanomater. 2012 (2012) 1–6.